Acta Biomaterialia 130 (2021) 161–171

Contents lists available at ScienceDirect

Acta Biomaterialia

journal homepage: www.elsevier.com/locate/actbio

Full length article

Biomimetic stiffening of cell-laden hydrogels via sequential thiol-ene and hydrazone click reactions

Chun-Yi Chang[a], Hunter C. Johnson[b], Olivia Babb[c], Melissa L. Fishel[c,d,e], Chien-Chi Lin[a,b,e,*]

[a] Weldon School of Biomedical Engineering, Purdue University, West Lafayette, IN, USA
[b] Department of Biomedical Engineering, Purdue School of Engineering & Technology, Indiana University-Purdue University Indianapolis, Indianapolis, IN, USA
[c] Department of Pediatrics, Indiana University School of Medicine, Indianapolis, IN, USA
[d] Department of Pharmacology and Toxicology, Indiana University School of Medicine, Indianapolis, IN, USA
[e] Indiana University Simon Comprehensive Cancer Center, Indianapolis, IN, USA

ARTICLE INFO

Article history:
Received 28 February 2021
Revised 11 May 2021
Accepted 24 May 2021
Available online 1 June 2021

Keywords:
Dynamic hydrogels
Hyaluronic acid
Cancer associated fibroblasts
Thiol-ene chemistry
Hydrazone reaction

ABSTRACT

Hydrogels with dynamically tunable crosslinking are invaluable for directing stem cell fate and mimicking a stiffening matrix during fibrosis or tumor development. The increases in matrix stiffness during tissue development are often accompanied by the accumulation of extracellular matrices (e.g., collagen, hyaluronic acid (HA)), a phenomenon that has received little attention in the development of dynamic hydrogels. In this contribution, we present a gelatin-based cell-laden hydrogel system capable of being dynamically stiffened while accumulating HA, a key glycosaminoglycans (GAG) increasingly deposited by stromal cells during tumor progression. Central to this strategy is the synthesis of a dually-modified gelatin macromer – gelatin-norbornene-carbohydrazide (GelNB-CH), which is susceptible to both thiol-norbornene photopolymerization and hydrazone click chemistry. We demonstrate that the crosslinking density of cell-laden thiol-norbornene hydrogels can be dynamically tuned via simple incubation with aldehyde-bearing macromers (e.g., oxidized dextran (oDex) or oHA). The GelNB-CH hydrogel system is highly cytocompatible, as demonstrated by *in situ* encapsulation of pancreatic cancer cells (PCC) and cancer-associated fibroblasts (CAF). This unique dynamic stiffening scheme provides a platform to study tandem accumulation of HA and elevation in matrix stiffness in the pancreatic tumor microenvironment.

Statement of significance

Hydrogels permitting on-demand and secondary crosslinking are ideal for mimicking a stiffening tumor microenvironment (TME). However, none of the current dynamic hydrogels account for both stiffening and accumulation of hyaluronic acid (HA), a major extracellular matrix component increasingly deposited in tumor stromal tissues, including pancreatic ductal adenocarcinoma (PDAC). The current work addresses this gap by developing a dynamic hydrogel system capable of simultaneously increasing stiffness and HA accumulation. This is achieved by a new gelatin macromer permitting sequential thiol-norbornene (for primary network crosslinking) and hydrazone click chemistry (for bioinert or biomimetic stiffening with oxidized dextran (oDex) or oHA, respectively). The results of this study provide new insights into how dynamically changing physicochemical matrix properties guide cancer cell fate processes.

© 2021 Acta Materialia Inc. Published by Elsevier Ltd. All rights reserved.

1. Introduction

The diagnosis and treatment of pancreatic ductal adenocarcinoma (PDAC) have not seen significant improvement over the past decades, in large part due to the complex and hypoxic tumor microenvironment (TME) [1–3]. A major hurdle to the treatment of PDAC is the dense and complex TME [4], which includes cellular (e.g., tumor cells, immune cells, pancreatic stellate cells (PSCs), and

* Corresponding author at: Thomas J. Linnemeier Guidant Foundation Endowed Chair & Professor, Department of Biomedical Engineering, Purdue School of Engineering & Technology, Indiana University-Purdue University Indianapolis, Indianapolis, IN 46202, USA.
E-mail address: lincc@iupui.edu (C.-C. Lin).

https://doi.org/10.1016/j.actbio.2021.05.054
1742-7061/© 2021 Acta Materialia Inc. Published by Elsevier Ltd. All rights reserved.

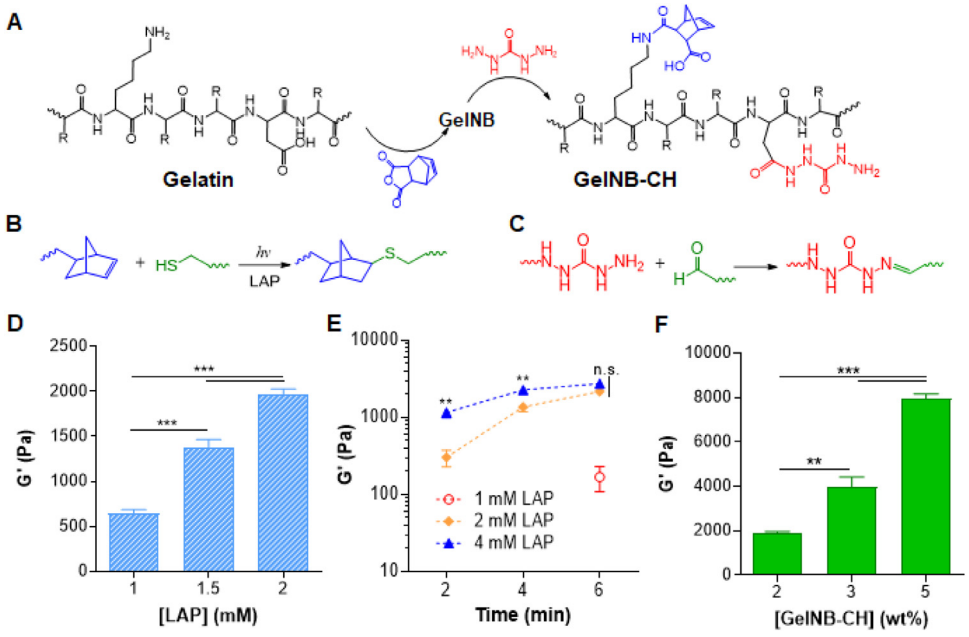

Fig. 1. Synthesis and crosslinking of GelNB-CH hydrogels. (A) Synthesis of GelNB and GelNB-CH. (B) Schematic of thiol-norbornene photo-click reaction. (C) Effect of photoinitiator LAP concentration on moduli of UV light (365 nm) crosslinked GelNB-CH/PEG4SH hydrogels. [GelNB-CH] = 5 wt%, [PEG4SH] = 1 wt% ($R_{SH/NB}$ = 0.5). UV light: 5 mW/cm^2 for 2 min. (D) Effect of visible light polymerization time and LAP concentration of crosslinking of GelNB-CH/PEG4SH hydrogels. [GelNB-CH] = 5 wt%, [PEG4SH] = 1 wt% ($R_{SH/NB}$ = 0.5). Visible light (400-700 nm): 70 kLux. (E) Schematic of hydrazone-click reaction. (F) Effect of macromer content on modulus of hydrazone hydrogels crosslinked by GelNB-CH and PEG4pAld ($R_{Ald/CH}$ = 0.5). Polymerization time: 30 minutes. Shear modulus of GelNB-CH gels was analyzed using one-way ANOVA with a Bonferroni post-test analysis.

cancer-associated fibroblasts (CAFs) [5]) and non-cellular components (e.g., cytokines and excess matrices) [6–8]. While the growth of primary cancer cells dictates the progress of PDAC development, stromal cells such as PSCs and CAFs are known to secrete a myriad of growth factors, cytokines, and extracellular matrices (ECM) that also contribute to tumor progression. The development of biomimetic tumor matrix will benefit the understanding of PDAC cell fate processes, which in turn will assist the development of anti-PDAC therapeutics.

Hydrogels are swollen three-dimensional (3D) networks of crosslinked hydrophilic polymers that enable strategic manipulation of physicochemical properties to mimic key aspects of ECM in healthy or diseased tissues [9,10]. For example, Matrigel, a tumor-derived matrix, is widely used to study cancer cell growth and to promote self-organization and functionality of stem cell derived organoids [11]. However, the compositions of Matrigel are ill-defined and batch-dependent, making it challenging in mechanistic interpretation of experimental results. Matrigel is also too compliant and cannot recapitulate the evolving mechanics in the stem cell niche or cancer stromal tissue. To that end, recent efforts have demonstrated that semi-synthetic hydrogels crosslinked by synthetic and modified natural macromers are highly useful for *in vitro* and *ex vivo* cancer cell research. The use of synthetic macromers and chemistries offers a facile means of tuning matrix mechanics, while the addition of biologically-derived macromers renders the matrix responsive to cells (e.g., adhesion and matrix degradation).

Hydrogels with dynamically tunable matrix properties (i.e., dynamic hydrogels) can mimic key aspects of TME [12–15]. Dynamic stiffening of cell-laden hydrogels are conventionally achieved by performing a secondary crosslinking within an existing hydrogel network. Various strategies have been employed to induce dynamic hydrogel stiffening, including photochemistry, supramolecular assembly, reversible protein folding, ionic crosslinking, and enzymatic reactions [16]. For example, we have reported poly(ethylene glycol) (PEG)-peptide hydrogels that could be dynamically stiffened via tyrosinase-mediated [17] or visible light initiated di-tyrosine crosslinking [14]. In particular, we synthesized gelatin-norbornene (GelNB) and further modified it with 4-hydroxyphenylacetic acid (HPA), yielding a dual functionalized GelNB-HPA. Hydrogels crosslinked by GelNB-HPA and thiolated HA (THA) could be dynamically stiffened by tyrosinase to mimic the increase in matrix stiffness during PDAC progression [17]. Using this modular and dynamic hydrogel system, we demonstrated a synergistic effect of matrix stiffening and the presence of HA on promoting epithelial-mesenchymal transition (EMT) in pancreatic cancer cells (PCCs). In a separate study, we showed that PCCs grown in a dynamically stiffened matrix acquired resistance to chemotherapeutic treatment [18], suggesting a critical role of matrix mechanics on drug sensitivity in cancer cells.

In the prior GelNB-HPA hydrogel system, HA was incorporated as part of the primary network that was subsequently stiffened by tyrosinase (i.e., no change in biochemical components). While hydrogel stiffness was effectively increased after secondary enzymatic crosslinking, this system did not resemble cancer progression where HA was increasingly deposited overtime [8]. To mimic a stiffening PDAC tissue with increased HA accumulation, we report here a new dynamic hydrogel system integrated with two click chemistries, namely thiol-norbornene photo-click reaction for the primary network crosslinking and hydrazone click reaction for the concurrent dynamic stiffening and HA accumulation. Central to this physicochemically relevant dynamic hydrogel was the synthesis of a NB and carbohydrazide (CH) dually functionalized gelatin (i.e., GelNB-CH, **Fig 1A**). The use of gelatin-based macromer conferred the hydrogel network with both cell adhesive ligands and protease-labile linkers, while the installation of NB and CH reactive handles permitted initial gelation either by photo-click thiol-norbornene reaction (**Fig. 1B**) [19] or by hydrazone click chemistry (**Fig. 1C**) [20]. The two orthogonal click chemistries were employed sequentially to yield cell-laden hydrogels susceptible to dynamic stiffening using oxidized polysaccharides (e.g., bioinert dextran or bioactive HA). While the use of oxidized dextran (oDex) did not in-

troduce bioactive component during/after stiffening, the utilization of oxidized HA (oHA) permitted a stiffened network with accumulation of HA, which mimics the matrix stiffening and increased deposition of HA during pancreatic cancer progression. In addition to evaluating the effect of secondary hydrazone-based click reaction on the dynamic stiffening of thiol-norbornene hydrogels, we tested the cytocompatibility of this new dynamic hydrogel system with PCC (e.g., PANC-1) and pancreatic CAF [21], which secretes cytokines and tumor ECM to support PCC growth. Using a bioinert macromer (i.e., stiffening with oDex) as a control, we further evaluated the effect of biochemically active dynamic stiffening (i.e., stiffening with oHA) on PCC and CAF phenotype, including cell proliferation and spreading, as well as expression of HA receptor CD44 and a panel of CAF associated proteins.

2. Materials and methods

2.1. Materials

Type B gelatin (bloom 225) was purchased from Electron Microscopy Sciences. Carbic anhydride (CA), carbohydrazide (CH) and 1-ethyl-3-(3-dimethylaminopropyl)carbodiimide HCl (EDC) were purchased from Acros Organics. Sodium hyaluronate (74 kDa) and dextran (20 kDa) were purchased from Lifecore Biomedical and Sigma-Aldrich respectively. Hydroxy benzotriazole (HOBt) was purchased from Oakwood Chemical**.** Poly(ethylene glycol)-tetra-propionaldehyde (PEG4pAld, 10 kDa) and PEG-tetra-thiol (PEG4SH, 10 kDa) were purchased from Layson Bio. α-chymotrpsin was purchased from Amresco. Hyaluronidase was purchased from Worthington Biochemical Corporation. Geltrex was purchased from Thermo Fisher Scientific. Anti-CD44 antibody and Alexa Fluor 488 donkey anti-mouse IgG was obtained from RayBiotech and Thermo Fisher Scientific, respectively. CAF marker antibody sampler kit was purchased from Cell Signaling. Live/dead viability kit was purchased from Biotium. High glucose DMEM was purchased from GE Healthcare. DPBS, fetal bovine serum (FBS), and antibiotic-antimycotic were purchased from Corning. All other chemicals were purchased from Sigma-Aldrich unless otherwise noted.

2.2. Macromer synthesis

GelNB was synthesized following a published procedure [19]. The substitution of NB group was characterized via Fluoraldehyde assay using unmodified gelatin with known concentrations as a standard. GelNB-CH was synthesized by dissolving GelNB in 50 mL PBS at 45 °C and stirred via a rotary evaporator. GelNB solution was then moved to an oil bath kept at 45 °C. CH was added to the solution and mixed until dissolved, followed by addition of EDC and HOBt dissolved in equal volume of ddH_2O and amine-free dimethylformamide (DMF) (total vol. 13 mL). The pH was adjusted to 5 and the reaction was allowed to proceed for 24-h at 45 °C. After 24-h, the solution was transferred to a dialysis membrane of 12–14 kDa molecular weight cut-off (MWCO), where it underwent dialysis against ddH_2O for 3-days at 40 °C. After dialysis, the solution was lyophilized to obtain the final product. Functionalization of CH was characterized via 2,4,6-trinitrobenzene sulfonic acid (TNBSA) assay using a standard curve created from adipic acid dihydrazide.

To synthesize oHA and oDex, $NaIO_4$ was first dissolved in 200 mL ddH_2O. HA (or dextran) was then dissolved into the $NaIO_4$ solution and stirred overnight in dark. The solution was transferred to a 4-6 kDa MWCO dialysis membrane and dialyzed against ddH_2O for 3-days, followed by freeze-drying to collect the final product. Theoretical functionalization was ascertained via concentration of diols that could be oxidized via ring-opening. The amounts of $NaIO_4$ used were calculated based on the concentration of diol per weight percent (independent of the molecular weight) of HA or dextran (i.e., 0.236 mg and 0.525 mg of $NaIO_4$ per mg of HA and dextran, respectively).

2.3. Hydrogel crosslinking and stiffening

Thiol-norbornene hydrogel crosslinking was performed via either light initiated photo-click reaction with lithium phenyl-2,4,6-trimethylbenzoylphosphinate (LAP) as the photoinitiator. GelNB or GelNB-CH, and thiol-containing macromers were mixed thoroughly with vortex and pipetted between two glass slides separated by 1 mm thick spacers, followed by either 365 nm light (5 mW/cm^2, Blak-Ray XX-15M UV Lamp) for 2 min or visible light (400-700 nm, 70 kLux, AmScope Cold-Light Source Haloid Lamp) exposure for various duration [22]. Hydrazone hydrogels were prepared by creating two precursor solutions, one with GelNB-CH and one with an aldehyde-containing macromer. The precursor solutions were mixed in an oxygen plasma treated glass slide and incubated for 30 minutes in a humidifying chamber. After gelation, hydrogel discs were punched out with an 8 mm biopsy punch and gels were incubated at least 1-hour in DPBS supplemented with antibiotics prior to rheological characterization. Stiffening was achieved by introducing soluble, aldehyde-containing cross-linkers (i.e., oHA, PEG4pAld, or oDex) to hydrogel swelling solution. Stiffening was initiated immediately following pre-stiffened rheological characterization and lasted for 24-h. Quantification of gel shear/storage modulus (G') and loss modulus (G'') was accomplished via a parallel plate in strain sweep mode and frequency sweep mode using Bohlin CVO 100 Digital Rheometer at room temperature. Strain range was from 0.1 – 5% at an oscillating frequency of 1 Hz over the course of 100 seconds. The values in the linear viscoelasticity region (LVE) were averaged to obtain G' and G''. Frequency sweep tests were conducted at an oscillating frequency range from 0.1 – 10 Hz at a constant strain of 10%. Strain of 10% was applied for stress relaxation analysis and relaxation modulus was tracked for 1000 s using MCR 102 rheometer (Anton Paar). Nuclear magnetic resonance (NMR) spectroscopy was performed to qualitatively verify the modification NB and CH on gelatin. Fourier-transform infrared (FTIR) spectroscopy was performed for gelatin, GelNB, GelNB-CH, oDex, and GelNB-CH hydrogels (soft and oDex-stiffened) using Nicolet iS 10 FTIR spectrometer (Thermo Fisher). Scanning electron microscopy (SEM) images were taken for non-stiffened and oDex-stiffened GelNB-CH gels using JSM-7800F field emission scanning electron microscope (JEOL).

2.4. Enzymatic degradation of GelNB-CH hydrogels

GelNB-CH hydrogels were either stiffened with 0.5 wt% oHA for 24 h (oHA-stiffened), or with 0.05 wt% oDex for 6 h (oDex-stiffened). The hydrogels were measured for storage modulus before subjected to enzymatic degradation. Specifically, cylindrical gels (diameter: 8 mm, thickness: 0.8 mm) were incubated in 2 mg/mL chymotrypsin at room temperature. Gel mass was measured gravimetrically every 10 min after removing excess solution on the hydrogel. Alternatively, gels were incubated in 1 mg/mL hyaluronidase at 37 °C, and gel mass was measured after 10 min, 30 min, 60 min, and every hour afterward.

2.5. Cell maintenance and encapsulation

PANC-1 cells and immortalized GFP-expressing CAF cells (labeled as CAF3 in the HYAL expression study) [21] were cultured on tissue culture plastics (TCP) in high glucose DMEM supplemented with 10% FBS and 1% antibiotics. Media was refreshed every 2 – 3 days and the cells were allowed to grow until they reached

70% confluence for passaging or encapsulation. Prior to encapsulation, all hydrogel precursor solutions were sterile-filtered through 0.22 µm syringe filters. Some materials, such as modified gelatin and HA, were exposed to germicidal mid-wave UV (i.e. 254 nm) for 30 min prior to use. Encapsulating PANC-1 cells and CAFs in hydrogels was accomplished in 1 mL syringes with their tops cut off for sample loading and gel retrieval. The volume of each hydrogel was 25 µL and the encapsulation cell density was 1×10^5 cells/mL for PANC-1 and 1×10^6 cells/mL for CAF. The gelation parameters were consistent with hydrogel fabrication for rheological characterization (i.e. 5 mW/cm^2 for 2-minutes). In selected experiments, the PANC-1-laden hydrogels were maintained in high glucose DMEM with 10% FBS or DMEM/F12 supplemented with 10 ng/ mL epithermal growth factor (EGF) and 20 ng/mL fibroblast growth factor (FGF) (i.e., spheroid medium). CAF-laden hydrogels were incubated in high glucose DMEM with 10% FBS. Media of cell-laden hydrogels were refreshed every 2 – 3 days. Stiffening was achieved by incubating hydrogels in aldehyde-containing cross-linkers (i.e., oHA or oDex) for 24 h, from day-1 to day-2. To reach a pathophy relevant stiffness, gels were either stiffened with 0.5 wt% oHA for 18 h followed by 0.05 wt% oDex for 6 h (oHA+oDex-stiffened), or alternatively, with 0.03 wt% oDex (oDex-stiffened).

The same cell density was used for cell encapsulation using Geltrex^{TM}, an LDEV-free reduced growth factor basement membrane matrix. Briefly, Geltrex solution was mixed with cell suspension below room temperature. The mixture was deposited to the surface of a well-plate and allowed to undergo gelation at 37°C as instructed by the manufacturer's protocol.

2.6. Characterization of cell viability, cell/spheroid size, and cell spreading

Qualitative characterization of cell viability and morphology were performed using live/dead staining. Calcein AM and Ethidium homodimer III were used for labeling live and dead cells, respectively. Hydrogels with encapsulated cells were transferred to new well plates and washed 3x with DPBS for 5-min prior to the addition of staining solution. Once staining solution was added, the gels were protected from light and incubated for 1-h on a shake plate. Excess stain solution was removed from the gels, followed by 3 times of 5-min DPBS washes. Finally, cell-laden hydrogels were transferred onto a glass slide for imaging via LionHeart FX automated microscope or a confocal microscope. Image analysis was conducted with ImageJ. To get a better resolution image of CAF, the live/dead image of CAF were converted to binary color before subjected to analysis.

2.7. RNA isolation, reverse transcription, and Real time quantitative PCR (qRT-PCR)

PANC-1 cells and three patient-derived CAFs (CAF19, CAF2, CAF3) [21,23] were collected while in log phase growth and RNA was extracted according to manufacturer's protocol using the Qiacube (Qiagen, Hilden, Germany, USA). Subsequently, cDNA was prepared from 1µg of total RNA in a 25 µl reaction mix (Applied Biosystems). qRT-PCR was performed using the SYBR Green PCR kit (Applied Biosystems, Foster City, CA, USA), with a final volume of 20 µL/well in 96-well plates on the CFX96 Real time PCR detection system (BioRad, Hercules, CA, USA). Primers for the HYAL1-3 genes were purchased from (Thermo Fisher Scientific, Waltham, MA, USA) with the sequence described in the literature [24]. qRT-PCR cycling conditions were: 1 min at 95 °C; 10 min at 95 °C; 15 s at 95 °C; 1 min at 60 °C for 40 cycles. The 2-ΔΔCT method was used to determine relative mRNA expression levels and the b-Actin gene was used as the reference gene. The expression of HYAL1-3 in PANC-1 cells were set to 1 and used to normalize the expression levels in CAFs.

2.8. Western blot analysis of protein expression

CD44 expression on PANC-1 was examined by immunofluorescence staining on day-8. Briefly, encapsulated cells were fixed, permeabilized, blocked, and incubated with diluted (1:100) anti-CD44 antibody (RayBiotech, #144-00340-100) overnight at 4 ncubated with diluted (1:200) Alexa Fluor 488 donkey anti-mouse IgG (H+L) (Invitrogen, #A-21206) overnight at 4 °C. Finally, the encapsulated cells were counter-stained with DAPI (1:1000) (AnaSpec, #AS-83210), followed by confocal microscopy to obtain z-stack images (400 µm thick, 20 µm per slice). Image analysis was conducted with ImageJ.

F-actin expression of CAFs was examined to visualize cytoskeletal structure in non-stiffened, oHA-stiffened, and oDex-stiffened hydrogels. Briefly, the encapsulated cells were fixed, permeabilized, and stained with rhodamine phalloidin solution (100 nM) (Cytoskeleton, # PHDR1) for 1 h at room temperature. Finally, the encapsulated cells were counter-stained with DAPI (1:1000). Cell imaging and analysis were conducted in the same manner as described for CD44 immunofluorescence staining.

Expression of six CAF-associated proteins (platelet-derived growth factor receptor (PDGFRα), PDGFRβ, fibroblast activation protein (FAP), α-smooth muscle actin (αSMA), vimentin, and S100A4) was analyzed through western blot. Briefly, soft (non-stiffened), oHA-stiffened and oDex-stiffened CAF-laden gels were digested with 100 U/mL collagenase for 1 h on day-8. CAFs were collected by centrifugation and washed three times with DPBS. To extract the CAF-associated proteins, cell lysis buffer was added to the collected CAFs and incubated on ice for 5 min before subjected to sonication. Total protein concentration was obtained through BCA protein assay (Pierce). Extracted protein was separated by SDS-PAGE, and transferred to a PVDF membrane. The blots were blocked and stained as described previously [25] with modification. Briefly, the membranes were incubated with 2% nonfat milk in PBST (PBS containing 0.05% Tween 20), followed by incubation in primary antibodies of the CAF-associated proteins (1:1000) and housekeeping protein (i.e., GAPDH) overnight at 4 °C. After washed with PBST, the membranes were incubated in HRP-conjugated secondary antibody (anti-rabbit IgG, 1:2000) at room temperature for 1 h. The blots were washed with PBST and treated with chemiluminescence detection kit (SuperSignal West Pico Detection Kit, Thermo Scientific). Immunoblotting images were obtained using a chemiluminescence imaging system (LAS3000, Fuji Film).

2.9. Antibody arrays for profiling the secretion of cytokines and MMP

To examine the effect of gel stiffening with oHA/oDex on CAF cytokine/MMP secretion, conditioned media of CAF from day-4 to day-6 were collected and subjected to antibody-based human inflammation array (RayBiotech, #AAH-INF-3-8), human growth factor array (RayBiotech, # AAH-GF-1-8), and human MMP array (RayBiotech, # AAH-MMP-1-8). The assays were carried out according to the manufacturer's instructions. Briefly, antibody membranes were blocked for 1 h at room temperature, incubated with conditioned media overnight, incubated with biotinylated antibody cocktail, and finally with HRP-streptavidin. The membranes were incubated with chemiluminescence detection buffer for 2 min before imaging with an imaging system (LAS3000, Fuji Film). Signal intensity of individual spots on the scanned membranes were quantified with ImageJ.

2.10. Statistical analysis

All numerical data analyses and statistical analyses were performed using GraphPad Prism software. Hydrogels were prepared in triplicate for mechanical testing. Cell studies were repeated at least twice for verification of results. Single, double, and triple asterisks represent $p < 0.05$, 0.01, and 0.001, respectively.

3. Results

3.1. GelNB-CH synthesis and dual-mode hydrogel crosslinking

GelNB-CH was synthesized via a two-step carbodiimide chemistry (**Fig. 1A**) and the modifications of NB and CH moieties on gelatin were confirmed by 1H NMR (**Fig. S1**). Using Fluoraldehyde assay and TNBSA assay, the degrees of substitution were determined to be ~50% for NB (ca. 2 mM NB per wt% macromer) and ~37% for CH (ca. 4 mM CH per wt% macromer), respectively. Gelatin, GelNB, GelNB-CH were also analyzed by FTIR but the results showed no significant difference among the three groups (**Fig. S2A**). These may be attributed to the low weight contents of the NB and CH moieties on the large GelNB-CH molecule. On the other hand, the peak at 1730 cm^{-1} of oDex spectrum corresponds to the stretching vibration of carbonyl group [26]. To evaluate gelation, GelNB and GelNB-CH macromers were subjected to either UV (365 nm) or visible light (400 – 700 nm) initiated thiol-norbornene gelation (**Fig. 1B**) [19,22,27]. Using 5 wt% GelNB-CH and 1 wt % PEG4SH ($R_{SH/NB} = 0.5$), we demonstrated tunable UV light initiated thiol-norbornene gelation with the new GelNB-CH macromer (**Fig. 1C**). At this gelatin content, hydrogel shear moduli (G′) increased as the concentration of photoinitiator LAP, ranging from ~0.7 kPa to ~ Pa for 1 to 2 mM LAP (**Fig. 1D**). We also tested the orthogonal thiol-norbornene gelation using visible light exposure (400-700 nm) at different photoinitiator concentrations (i.e., 1, 2, or 4 mM LAP). In general, higher LAP concentration led to gels with higher G′ at the same polymerization time. However, with 1 mM LAP no gel was formed until after 6 min of visible light exposure (**Fig. 1E**). Under the same macromer compositions and polymerization time, gels formed with 4 mM LAP were significantly stiffer than those crosslinked with 2 mM LAP. No significant difference was found after 6 min of polymerization for macromers containing 2 mM or 4 mM LAP, suggesting that the gels had reached maximum degree of crosslinking (G′ ~ 2.1 kPa & 2.7 kPa for 2 mM & 4 mM LAP, respectively). Note that G′ reported in **Fig. 1D** and **1E** were from gels crosslinked with twice as many norbornene groups as the thiols (i.e., $R_{SH/NB} = 0.5$). At $R_{SH/NB}$ of 1, hydrogels were crosslinked to an even higher G′ (~10 kPa. **Fig. S3**), confirming the high efficiency of thiol-norbornene gelation using the new GelNB-CH macromer.

The CH moiety on GelNB-CH provided an alternate crosslinking mechanism via hydrazone-click chemistry (**Fig. 1C**). Specifically, CH could 'click' with macromers containing aldehyde groups, including many oxidized polysaccharides (e.g., HA, dextran, etc.) or aldehyde-modified multi-arm PEG (e,g., PEG4pAld). We demonstrated this gelation mechanism by using GelNB-CH and PEG4pAld (**Fig. 1F**), where higher concentration of GelNB-CH led to stiffer hydrazone gels. Specifically, after 30 min of gelation to ensure complete crosslinking, G′ of the hydrazone hydrogels reached ~2, 4, and 8 kPa, respectively, for 2, 3, and 5 wt% GelNB-CH ($R_{Ald/CH} = 0.5$). Of note, all hydrazone click hydrogels exhibited significant stickiness (data not shown), potentially caused by the reversible hydrazone bonding. While GelNB-CH permits dual mode crosslinking (i.e., thiol-norbornene and hydrazone click reaction), we chose thiol-norbornene photo-click chemistry in the subsequent studies for its rapid and efficient crosslinking.

3.2. Dynamic hydrogel stiffening via hydrazone-click chemistry

We demonstrated dynamic hydrazone stiffening in the primary GelNB-CH/PEG4SH thiol-norbornene hydrogels with G′ (~2 kPa) similar to the stiffness of healthy pancreatic tissues [6]. Upon incubation in 0.1 wt% oDex solution (**Fig. 2A**), G′ of the hydrogels rapidly increased from ~2200 Pa to ~24,000 Pa over 24 hours and gradually reached plateau at ~30,000 Pa after 72 h (**Fig. 2B**). Loss moduli (G′′) also increased over time but reached plateau at ~ 500 Pa (**Fig. 2B**). The secondary hydrazone bonding did not increase the viscoelasticity of the hydrogels, as demonstrated from the frequency sweep rheometry (**Fig. S4A, S4B**) and stress-relaxation curve (**Fig. S5**). To gauge whether hydrazone-stiffening can be achieved in a step-wise, temporally controlled manner, we incubated GelNB-CH hydrogels in oDex solution (0.1 wt%) intermittently. As expected, hydrogels were stiffened effectively only when the gels were placed in the oDex solution (**Fig. 2C**).

We next examined dynamic hydrazone-mediated stiffening using different aldehyde-containing macromers, including PEG4pAld (**Fig. S6**), oDex (**Fig. 2D, 2E**), and oHA (**Fig. S7**). Specifically, after incubation in 0.25 wt% PEG4pAld solution for 24 h, G′ increased from ~2 kPa to ~6 kPa (**Fig. S6**). oDex and oHA can be prepared with different degree of substitution and the degree of stiffening was a function of both the extend of oxidation (i.e., ~2 to 3-fold increase with 20% to 60% modified oDex, and ~1.3 to 7-fold increase with 20% to 100% modified oHA, respectively. **Fig. 2D, S7A**) and concentration of the stiffening reagent (**Fig. 2E, S7B**). It is worth noting that the stiffening effect of oDex is the highest among all stiffening reagents, with gel stiffness increased over 13-fold with merely 0.1 wt% of oDex (**Fig. 2E**), whereas gel stiffness only increased ~1.5-fold using the same concentration of oHA (**Fig. S7B**). The effect of oDex-mediated hydrazone stiffening was revealed using SEM, where the images show a decrease in pore size of the lyophilized hydrogel (from 10–15 μm to 5–10 μm. **Fig. 2F**). On the other hand, FTIR analysis results did not reveal difference between non-stiffened and oDex-stiffened GelNB-CH hydrogels (**Fig. S2B**).

3.3. Enzymatic degradation of dynamically stiffened hydrogels

Chymotrypsin and hyaluronidase were used to assess enzymatic degradation of GelNB-CH hydrogels, which were stiffened to similar G′ (**Fig. 3A**) by oDex alone (i.e., protease-degradable but insensitive to hyaluronidase) or with oHA (i.e., sensitive to both protease and hyaluronidase). During the 40 min chymotrypsin incubation, non-stiffened gels lost half of the mass due to protease-mediated degradation and the gels were completely degraded after 50 min of incubation (**Fig. 3B**). On the other hand, the mass of oHA- and oDex-stiffened hydrogels increased in the first 30-40 min of incubation and started to lose mass rapidly afterward. The oHA-stiffened gels and oDex-stiffened gels lost 38% and 34% of mass after 50 min of degradation, after which they became too soft to be retrieved for weight measurements. Similarly, hyaluronidase was used to digest gels that were either non-stiffened (soft), stiffened by oDex (for 6 h), or by oHA for 24 h (to ensure similar crosslinking density of the two groups prior to the start of the degradation. **Fig. 3A**). As expected, hyaluronidase did not degrade non-stiffened and oDex-stiffened gels over the course of 5 h incubation (**Fig. 3C**). On the other hand, gels stiffened with oHA were more susceptible to hyaluronidase-mediated degradation and lost ~13% mass after 5 h of incubation.

3.4. Effect of dynamic stiffening on PDAC cell fate

Prior to demonstrating the ability of the new GelNB-CH hydrogel system to recapitulate the dynamic tumor matrix, we encapsu-

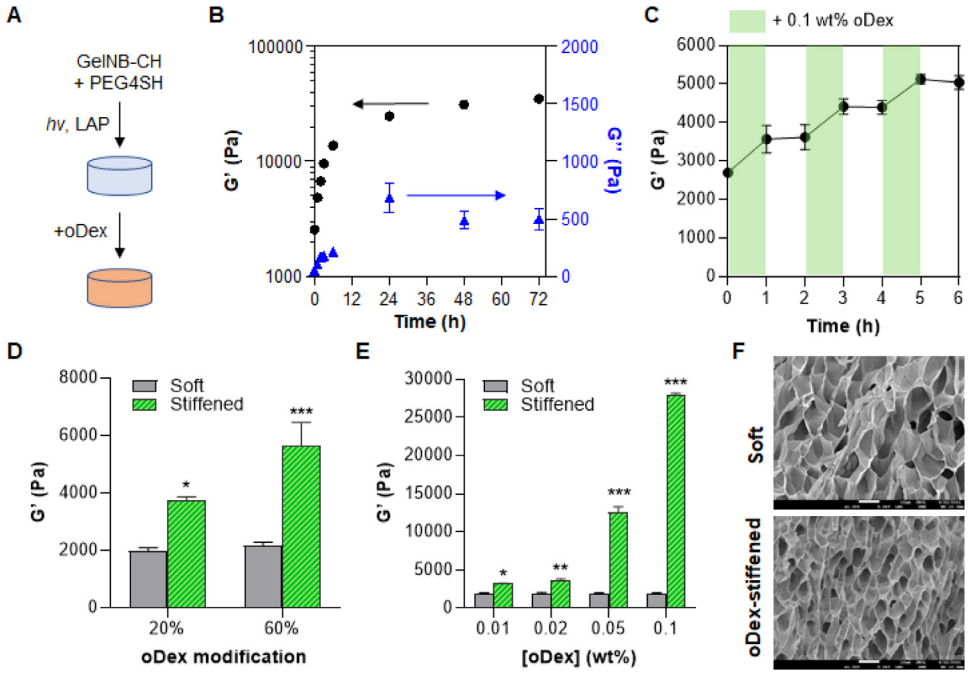

Fig. 2. Dynamic stiffening of thiol-norbornene hydrogels by secondary hydrazone crosslinking. (A) Schematic of gelation and stiffening. (B) Moduli of thiol-norbornene hydrogels during secondary hydrazone stiffening (+0.1 wt% oDex). (C) Shear moduli of hydrogels via step-wise stiffening. Gels were stiffened by intermittent incubation with 0.1 wt% oDex (shaded areas). (D) Effect of oDex functionality on the degree of stiffening. (E) Effect of oDex content on the degree of stiffening. All hydrogels were crosslinked by thiol-norbornene photopolymerization (365 nm, 5 mW/cm^2) with 5 wt% GelNB-CH and 1 wt% PEG4SH ($R_{thiol/NB}$=0.5, 2 mM LAP, 2 min light exposure. Shear modulus (D and E) of soft (non-stiffened) and oDex-stiffened was analyzed using two-way ANOVA with a Bonferroni post-test analysis. (F) SEM image of freeze-dried non-stiffened (soft) and oDex-stiffened GelNB-CH gels (scale: 10 μm).

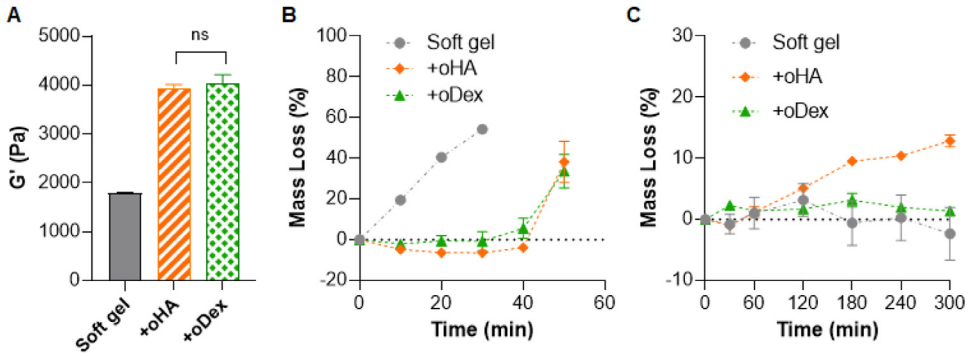

Fig. 3. Enzymatic degradation of GelNB-CH hydrogels. (A) Moduli of soft (non-stiffened) and hydrogels stiffened by oHA or oDex. (B) Chymotrypsin-mediated (2 mg/mL) degradation and mass loss of soft (non-stiffened) and hydrogels stiffened by oHA or oDex. (C) Hyaluronidase-mediated (1 mg/mL) degradation and mass loss of soft (non-stiffened) and hydrogels stiffened by oHA or oDex. Shear modulus (A) of oHA-stiffened and oDex-stiffened gels were analyzed using unpaired t-test.

lated PANC-1 cells in Geltrex, a version of Matrigel with reduced growth factors. As expected, the soft Geltrex matrix supported rapid growth of PANC-1 cells and formation of large amount of cell spheroids (**Fig. S8A, S8C**). In the GelNB-CH hydrogels, PANC-1 cells formed small multi-cell spheroids at day 2. Following 24 h of dynamic bioinert stiffening (i.e., oDex-stiffened) or biomimetic stiffening with HA accumulation (i.e., oHA-stiffened), the encapsulated PANC-1 cells also grew into spheroids and remained viable without significant difference in cell viability regardless of stiffening conditions (Fig. 4**A**). Furthermore, the spheroid size were similar between oHA-stiffened and oDex-stiffened (**Fig. S9A, S9B**). However, the cell spheroids density in oDex-stiffened hydrogels was higher than that of oHA-stiffened hydrogels, despite the similar stiffness between the two sets of dynamically-stiffened hydrogels. Interestingly, PANC-1 spheroids in non-stiffened and oHA-stiffened gels developed into a more mesenchymal-like morphology, especially in oHA-stiffened gels incubated in spheroid medium that contained EGF and FGF. The same irregular cell spheroid shape was not observed in oDex-only-stiffened gels (Fig. 4**B**). On day-8, the PANC-1 spheroids in stiffened gels were partially stained positive for EdU, indicating that cell proliferation was not inhibited by the stiffening (Fig. 4**C**). EdU+ cells were more concentrated in oDex-stiffened gels, whereas EdU+ staining was more evenly distributed in oHA-stiffened gels. In addition, CD44 staining results showed that its expression in PANC-1 spheroids was higher in oHA-stiffened gels than in oDex-stiffened ones (Fig. 4**D**), suggesting that the cells were responsive to the addition of HA after matrix stiffening.

3.5. Effect of dynamic stiffening on CAF phenotype

Human CAFs isolated from PDAC tumors were used to understand the effect of bioinert stiffening or biomimetic HA-mediated stiffening on stromal cell phenotype. All hydrogels supported the growth and spreading of pancreatic CAF (Fig. 5**A, B, C**). CAFs in

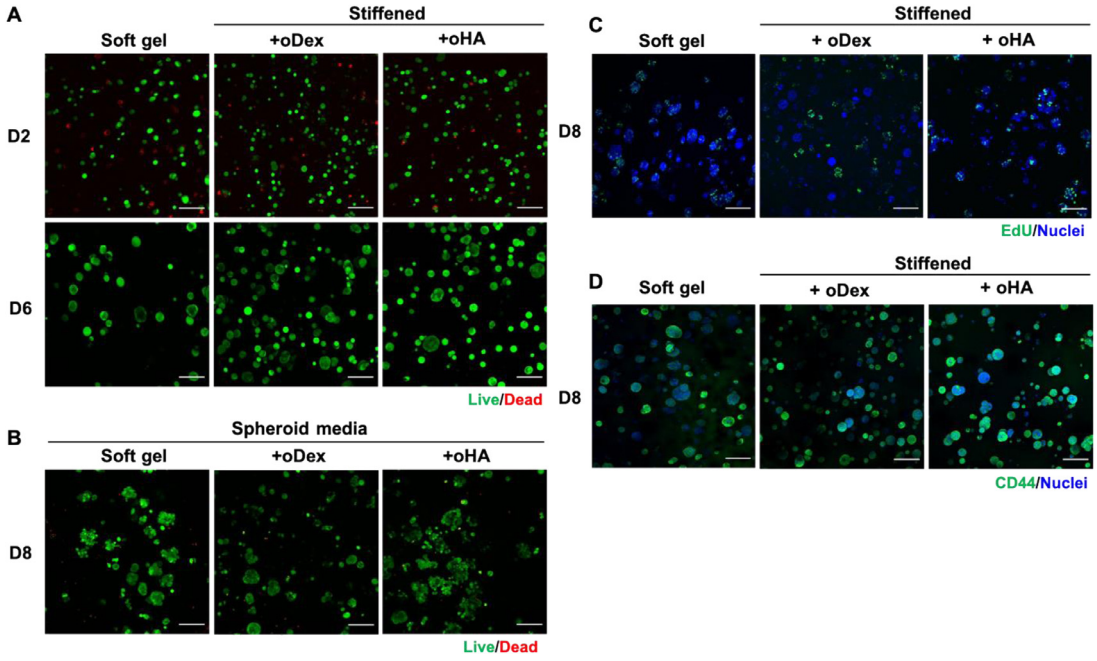

Fig. 4. Effect of dynamic stiffening on PANC-1 cell viability. (A) Live/dead staining of encapsulated PANC-1s in non-stiffened/oDex-stiffened/oHA-stiffened on day-2 and day-6. (B) Live/Dead staining of encapsulated PANC-1s in non-stiffened/oDex-stiffened/oHA-stiffened gels incubated in spheroid media on day-8. (C) EdU staining of encapsulated PANC-1s in oDex-stiffened and oHA-stiffened gels on day-8. (D) CD44 staining of encapsulated PANC-1s in oDex-stiffened and oHA-stiffend on day-8. Scale: 200 μm.

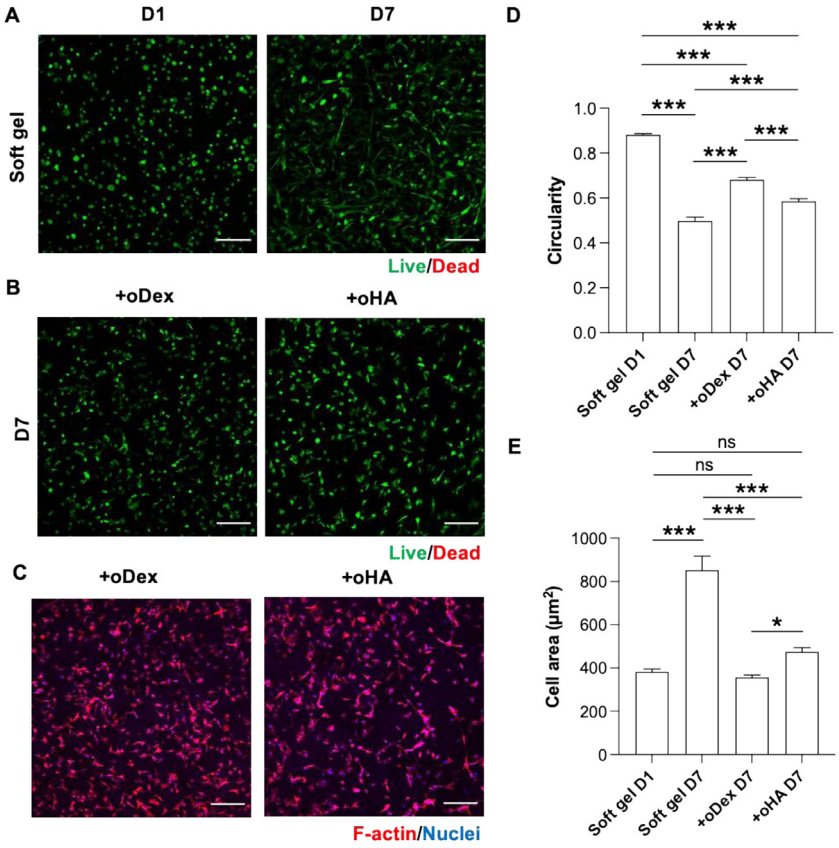

Fig. 5. Effect of stiffening on CAF cell phenotype. (A) Live/dead staining of CAFs in non-stiffened gels on day-1 and day-7. Scale: 200 μm. (B) Live/dead staining of CAFs in oDex-stiffened and oHA-stiffened gels on day-7. Scale: 200 μm. (C) F-actin staining of CAFs in oDex-stiffened and oHA-stiffened gels on day-8. Scale: 200 μm. (D) Quantified circularity of CAFs in soft (day-1 and day-7), oDex-stiffened (day-7), and oHA-stiffened (day-7). (E) Quantified cell area of CAFs in soft (day-1 and day-7), oDex-stiffened (day-7), and oHA-stiffened (day-7). (soft gel D1: n = 395, soft gel D7: n = 241, +oDex D7: n = 419, +oHA D7: n = 269).

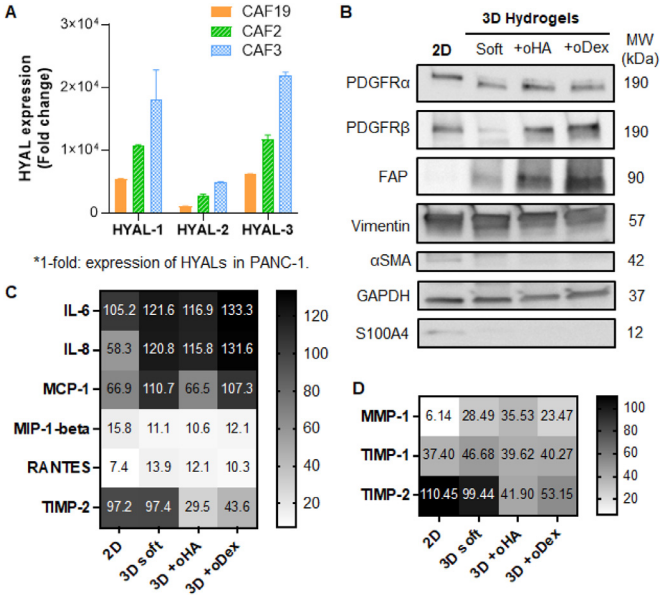

Fig. 6. Effect of stiffening on cytokine secretion from CAF. (A) HYAL1 – 3 expression of CAF19, CAF2, and CAF3 (B) Western blot of CAF-associated proteins extracted from CAFs in 2D, non-stiffened, oHA-stiffened, and oDex-stiffened gels (C) Quantified expression of select proteins in the inflammation array of CAF conditioned media (i.e., 2D, 3D soft, 3D +oHA, and 3D +oDex) (D) Quantified expression of select proteins in the MMP array of CAF conditioned media (i.e., 2D, 3D soft, 3D +oHA, and 3D +oDex).

non-stiffened GelNB-CH hydrogels exhibited high degree of mesenchymal spindle morphology (**Fig. 5A**), as revealed in the significant reduction of circularity (**Fig. 5D**) and more than double of cell area (**Fig. 5E**) after 7 days of culture. This was similar to the morphology of CAFs observed in Geltrex matrix (**Fig. S8B, S8D**). On the other hand, the spreading morphology was largely suppressed in both oDex and oHA-stiffened hydrogels (**Fig. 5B, 5D**). F-actin staining and converted live/dead images show that CAFs in oHA-stiffened hydrogels were more elongated than that in the oDex-stiffened gels (**Fig. 5C, S10**), as shown in the significantly lower circularity (**Fig. 5D**) and larger cell area (**Fig. 5E**). The increase in cell spreading may be attributed to higher levels of protease or hyaluronidase expression. Using qRT-PCR, we evaluated the expression of three hyaluronidases (i.e., HYAL-1, 2, 3) in 4 cell lines, including PANC-1 and three patient-derived CAFs (CAF19, CAF2, and CAF3). We found that the expression of HYALs in PANC-1 was low but several orders of magnitude higher in the three CAF lines examined (**Fig. 6A**), especially in CAF3, the cells used in the current GelNB-CH hydrogel encapsulation study. Western blot analysis of a panel of CAF-associated proteins showed that FAP expression was significantly upregulated in cells grown in 3D hydrogels, especially in the oHA and oDex-stiffened gels (**Fig. 6B**). On the other hand, the expression of S100A4 was visually detectable in 2D culture but not in cells cultured in all 3D hydrogels regardless of the stiffening condition (**Fig. 6B**).

3.6. Effect of dynamic stiffening on CAF secretory profiles

We further collected CAF conditioned media (CM) from different culture conditions (i.e., 2D, 3D soft, 3D +oHA, and 3D +oDex) and subjected them to antibody-based inflammation array, growth factor array, and MMP array analyses (**Fig. 6C, D, Fig. S11-S13**). Of note, proteins with low expression levels in all conditions (e.g., lower than 10 pixel intensity) were excluded in the data presentation**.** Cytokine array results show that interleukin 6 (IL-6), IL-8, and RANTES (regulated on activation normal T cell expressed and secreted) were all upregulated in 3D culture as compared to 2D culture, whereas macrophage inflammatory protein 1 beta (MIP1-β) was slightly downregulated in 3D culture. Interestingly, TIMP-2 was expressed less in stiffened gels, whereas monocyte chemoattractant protein 1 (MCP-1) was expressed higher in non-stiffened and oDex-stiffened gels, but not in oHA-stiffened gels (**Fig. 6C**). Results of MMP array show upregulation of MMP-1 secretion form CAF in 3D hydrogels (**Fig. 6D**). CAF in all conditions express similar amount of TIMP-1, while TIMP-2 expression was consistent with that from the inflammation array result (**Fig. 6C**). Results of growth factor array show that insulin-like growth factor binding protein 4 (IGFBP-4) and IGFBP-6 were highly expressed in all groups but the expression of IGFBP-3 was downregulated in 3D as compared to that in 2D culture (**Fig. S13**. It is worth noting that the expression of heparin-binding EGF-like growth factor (HB-EGF), stem cell factor receptor (SCF R), and transforming growth factor beta 2 (TGF-β2) were higher in 3D stiffened gels than in 2D culture and 3D non-stiffened gels. Furthermore, multiple growth factors and their receptors were expressed highest in 3D oDex-stiffened hydrogels, including fibroblast growth factors (FGFs), IGF-I, insulin-like growth factor 1 soluble receptor (IGF-I SR), macrophage colony-stimulating factor (M-CSF), placental growth factor (PlGF), SCF, and vascular endothelial growth factor D (VEGF D). Finally, the expression of MCSF R, neurotrophin-3 (NT-3), NT-4, TGF-β3, and VEGF Rs were highest in oDex-stiffened gels, followed by oHA-stiffened gels, non-stiffened gels, and 2D culture (**Fig. S13**).

4. Discussion

Tumor matrix-derived hydrogels (e.g., Matrigel, Geltrex) are commonly used for *in vitro* and *ex vivo* cancer cell culture. Indeed, we found that PANC-1 cells formed multi-cellular spheroids readily in the Geltrex matrix and small PANC-1 cell spheroids were observed as early as day-1 post encapsulation (data not shown). However, the stiffness of Geltrex matrix was not tunable and much softer ($G' < 1$ kPa) than that found in the PDAC tumor matrix ($G' \sim 4$ kPa) [6,28]. It is also impossible to dynamically introduce HA to the cell-laden Geltrex hydrogels. HA, a non-sulfated glycosaminoglycan, has been extensively used for fabricating hydrogels to study cancer cell fate [29–32]. As tumor progresses, HA is increasingly accumulated in various tumor microenvironments [33–36]. Fisher et al. created HA hydrogels with matrix metalloproteinases (MMP)-cleavable site for investigating breast cancer cell invasion [30]. Gurski et al. fabricated HA hydrogels through the formation of hydrazone bond for evaluating cancer drug efficacy [32]. The accumulation of HA has been shown to increase cancer cell proliferation, migration, and invasion [37]. The abundance of water-imbibing HA also acts as a physical barrier to increase interstitial fluid pressure, leading to reduced drug penetration and efficacy [7,8]. Although HA-based hydrogels have recapitulated the abundance of HA in TME, the accumulation of HA in TME is a dynamic process and this aspect has not been addressed in the development of dynamic hydrogels for cancer cell research.

Extracted from collagen, gelatin is widely used for tissue engineering applications owing to its cell adhesive ligands (e.g., RGD) and protease sensitivity. Since pure gelatin forms weak physical crosslinks only at low temperature, chemical modification is necessary to permit its covalent crosslinking into stable matrices for 3D cell culture. In this regard, our lab has reported the first norbornene-modified gelatin (i.e., GelNB) for orthogonal crosslinking of biomimetic and enzyme responsive hydrogels suitable for studying the impact of matrix physicochemical properties on pancreatic cancer cell behavior [19]. GelNB may be modified with additional reactive 'handle' (e.g., HPA) to permit secondary reaction within the primary thiol-norbornene hydrogel network. We have previously reported the synthesis and crosslinking of GelNB-

HPA hydrogels to probe the effect of dynamic matrix stiffening (induced by tyrosinase-mediated HPA dimerization) on pancreatic cancer cell growth and EMT [38,39]. While this approach was adequate for stiffening of cell-laden hydrogels, the use of tyrosinase may result in undesired crosslinking of natural tyrosine residues exposed on the surface of cells or proteins. To circumvent this potential issue, we designed another GelNB derivative, GelNB-CH, which is crosslinkable by thiol-norbornene click reaction and hydrazone bonding (**Fig. 1A**). This approach was inspired by an earlier study by Ito et al., where carbohydrazide-modified gelatin was used for Schiff's Base crosslinking with aldehyde-modified HA [20]. In that study, however, the moduli of the resulting gelatin/HA hydrogels were quite low (0.1–1 kPa). In this study, we show a diverse range of crosslinking reactions using the new GelNB-CH macromer (**Fig. 1**). Of note, cytocompatible long wavelength UV light (365 nm) initiated crosslinking resulted in gels with faster crosslinking kinetics and higher shear moduli under the same light exposure time and macromer formulation owing to the efficient thiol-norbornene reaction and high molar absorbability of LAP at 365 nm (~218 M^{-1} cm^{-1}) [27]. The use of visible light for initiation was less effective and required longer gelation time since LAP only absorbs weakly at the visible light wavelengths (~30 M^{-1} cm^{-1} at 405 nm) [38].

The addition of NB handle offers a multitude of methods for which one may use to form a primary network or to induce dynamic stiffening of gelatin-based hydrogels, including secondary thiol-norbornene click reaction [40] and tetrazine-norbornene inverse-electron demand Diels-Alder (iEDDA) click reaction [41,42]. On the other hand, the immobilized CH moiety allows dynamic stiffening of GelNB-CH hydrogels through hydrazone click chemistry. For this study, we used thiol-norbornene chemistry to crosslink the primary cell-laden hydrogels, while the secondary stiffening was achieved by hydrazone click reaction via diffusing in aldehyde-containing macromers. All macromers led to significant stiffening, with oDex being the most effective and economically friendly stiffening reagent (**Fig. 2**), followed by PEG4pAld (**Fig. S6**) and oHA (**Fig. S7**). As expected, the degree of gel stiffening scales with the concentration and the degree of functional group modification of the same stiffening reagent (e.g., **Fig. 2**). However, there is no negative correlation between the size (i.e., hydrodynamic radius: R_H) of the stiffening reagent and the degree of stiffening. For example, while the smaller PEG4pAld (10 kDa; R_H ~ 3.5 nm, extrapolated from literature values) [43] was more effective in stiffening GelNB-CH hydrogels than the larger oHA (74 kDa; R_H ~ 6.5 nm, estimated using values for dextran with an equivalent molecular weight) (**Fig. S6, S7**) [44], we did not find significant difference between the level of stiffening using 14.8 kDa and 74 kDa oHA (data not shown). Furthermore, when comparing stiffening using PEG4pAld and oDex that have a similar R_H (3.2 nm for PEG4pAld and 3.5 nm or oDex, respectively) [44], oDex was even more effective in gel stiffening than PEG4pAld (**Fig. 2, S6**). These phenomena suggest that diffusion is not the limiting factor governing the degree of stiffening and that other factors might contribute to the overall level of stiffening. It has been reported that gelatin could undergo phase separation with dextran [45–47] and the mixture of these two macromers may increase the chain rigidity of oDex, hence contributing to the ultra-high degree of stiffening. Nonetheless, the current studies have established a highly effective stiffening strategy oDex that may be implemented in other dynamic hydrogel systems.

Since all three macromers used in this study (i.e., gelatin, dextran, and HA) were susceptible to enzymatic degradation, we assessed the degradation of these hydrogels using chymotrypsin and hyaluronidase (**Fig. 3**). Chymotrypsin, a pancreas secreted enzyme, effectively cleaves C-terminal peptide bonds following tyrosine, tryptophan, and phenylalanine. Alternatively, hyaluronidase was used due to its ability to degrade HA. The gel degradation results revealed that the non-stiffened GelNB-CH gels were readily degraded by chymotrypsin and oDex-stiffened hydrogels degraded slower. The oDex-stiffened gels gained ~13% of the original gel mass in the first 1 h of incubation. This can be attributed to a tightened network structure that impeded the loss of degraded polymers, as well as increased water uptake after partial network degradation. For hyaluronidase-mediated gel degradation, hydrogels stiffened with oHA degraded faster than those stiffened with pure oDex since no HA was accumulated in the oDex-stiffened network. Furthermore, the hydrogels were not completely degraded since these gels composed primarily of thiol-norbornene crosslinks that were not susceptible to hyaluronidase. Of note, the purpose of these bulk scale gel degradation studies was not meant to mimic cell-secreted enzymatic matrix cleavage, which occurs locally nearby the cells. Rather, we were verifying that the hydrogels were susceptible to chymotrypsin and hyaluronidase, two enzymes found in the pancreatic tissue microenvironment.

Our data indicates that PANC-1 spheroids formed 3D spheroid-like clusters with distinct boundaries when cultured in soft hydrogels, indicating strong cell-cell adhesion (**Fig. 4**). On demand gel stiffening with oHA led to cell behavior that was different from bioinert stiffening with pure oDex (**Figs. 4–6**). Unlike dextran, a bioinert material that does not interact with pancreatic cancer cells, HA binds to CD44 and RHAMM and activates downstream signaling [48,49]. Gel stiffening using oHA is, therefore, considered "biomimetic stiffening", which enables both stiffening of the gel matrix and bioactive moieties for cell-ECM interaction. In general, biomimetic HA-mediated stiffening led to more mesenchymal-like phenotype, as well as higher proliferation and CD44 expression (**Fig. 4**), especially with the use of spheroid medium, a formulation designed for generating tumor spheroids in low adherence culture flask [50]. Spheroid medium contains epidermal growth factor (EGF) and FGF, both of which facilitate EMT [51,52]. Some PANC-1 spheroids with mesenchymal-like morphology can also be found in the non-stiffened gels, whereas the PANC-1 spheroids in oDex-stiffened gels were more compact. The binding between CD44 and HA has been reported to contribute to the mechanosensing and invasive phenotype of human glioblastoma cells [53,54]. The difference in PANC-1 morphology could be the result of a synergistic effect of the growth factors (i.e., EGF and FGF) in the spheroid medium and the mechanosensing through the binding between CD44 and HA. PANC-1 cells in oHA-stiffened gels were more proliferative than in their oDex counterpart, suggesting a role of HA-CD44 binding on enhancing cancer cell proliferation [55]. Although CD44 expression of PANC-1s was higher in oHA-stiffened gels as compared to oDex-stiffened gels, no research has indicated the causal link between HA and the expression of CD44 in the encapsulated cells. This finding raised the question of whether this phenomenon was a result of the difference in proliferation, or due to other reasons. Further investigation is required to identify the underlying mechanisms.

CAF-laden Geltrex gels started to degrade on day-3, thus Geltrex is not suitable for long term culture. In the soft, non-stiffened GelNB-CH hydrogels, CAF exhibited spindle shape and elongated morphology (**Fig. 5**), while PANC-1 cells formed multicell spheroids (**Fig. 4**). After stiffening, CAFs in oHA-stiffened gels were more spread out than that in the oDex-stiffened gels (**Fig. 5, S10**), despite the gels having similar moduli after stiffening (**Fig. 3**). This was likely a result of local matrix degradation by the upregulation of HYAL1-3 from CAFs, as revealed by the qRT-PCR results (**Fig. 6A**). Surprisingly, dynamic stiffening did not increase αSMA expression in CAFs (**Fig. 6B**). On the other hand, PDGFRβ was expressed more in 2D or stiffened gels than in non-stiffened ones, suggesting a potential stiffness-dependent PDGFR expression. Nielson et al. found a higher PDGFR expression in juxtatumoral CAFs

than CAFs in the periphery in the regressive stroma of PDAC [56]. Kim et al. reported that higher level of PDGFR expression in CAFs was associated with shorter survival from breast phyllodes tumor [57]. In addition, Pietras et al. revealed that inhibition of PDGFRs suppressed the expression of FGF-2 and FGF-7 in a mouse model of cervical carcinogenesis [58], although we did not observe a decrease in FGF-7 secretion in our growth factor result (**Fig. S13**). Collectively, the increased matrix stiffness in PDAC TME might contribute to PDAC tumor growth through a pathway that involves the expression of PDGFR in CAFs. From the Western Blot results, we found a higher expression of FAP in 3D matrix, especially in the stiffened gels (**Fig. 6B**), indicating that CAFs may be more cancer-promoting in the dynamically stiffened gels [59]. Interestingly, no S100A4 expression was detected in CAFs grown in 3D hydrogels, regardless of stiffening conditions. It has been reported that S100A4 expression in CAF was lower at the invasive front than the intratumoral stroma of colorectal cancer, and the expression decreased significantly as the disease progressed [60]. Hence, the decreased S100A4 expression in 3D hydrogels is another indicator that CAFs were more cancer-promoting in 3D culture and that 2D culture of CAFs is inadequate in studying their activation.

CAFs are known to be a source of various cytokines and growth factors, which led to our interest in understanding the effect of gel stiffening with biomimetic or bioinert polymer on the secretion of those cytokines and growth factors. Ohlund et al. demonstrated that there are distinct populations of CAFs within co-cultures and characterized the αSMA^{low} IL-6^{high} expressing CAFs as inflammatory CAFs (iCAFs) and αSMA^{high} IL-6^{low} expressing CAFs as myofibroblastic CAFs (myCAFs) [61]. Our data shows that IL-6 was upregulated in 3D hydrogels than in 2D culture, suggesting that biomimetic hydrogel culture may enhance the inflammatory properties of the CAFs. We also show that TIMP-2 expression was comparable in 2D culture and 3D soft hydrogels. However, it was downregulated in both stiffened groups, especially in the oHA-stiffened hydrogels (**Fig. 6C, D**). TIMP-2, an inhibitor for soluble MMP-2 and membrane-bound MMP14, has a suppressing effect on invadopodia formation in PDAC cells [62]. The upregulation of MMP-1 and suppression of TIMP-2 expression from CAFs in the oHA and oDex-stiffened hydrogels suggests that a stiffening microenvironment may lead to protease-mediated PCC migration and invasion. While current study did not include PCC/CAF co-culture experiments, the findings presented herein provide several interesting directions for future exploration of PCC/CAF co-culture in dynamic hydrogels.

5. Conclusion

Based on sequential thiol-norbornene and hydrazone click reactions, we have established new cell-laden dynamic hydrogels with the ability to simultaneous increase matrix stiffness and HA accumulation. The newly synthesized GelNB-CH is adaptable for both light mediated crosslinking and hydrazone-based gelation. When crosslinked by photo-click thiol-norbornene reaction, the hydrogels could be further stiffened with aldehyde-bearing macromers, including bioinert oDex and bioactive oHA. These new dynamic hydrogels mimic a key aspect of the pancreatic tumor stromal microenvironment, as it permits the accumulation of HA during matrix stiffening. We show that cancer and stromal cells responded differently to the biomimetic stiffening matrix, including changes in morphology, protein expression, and secretion of cytokine/growth factors. Gel stiffening with “bioactive” stiffening reagent, oHA, led to higher CD44 expression and a higher percentage of proliferating cells in PDAC-1 spheroids. 3D culture overall, and in particular gels with dynamic stiffening, lead to more invasive CAF morphology, in part due to higher expression of HYALs and suppression of TIMP-2 secretion. The new dynamic hydrogel system presented in this study should facilitate the investigation of cell-cell and cell-matrix interactions in various cancer types.

Declaration of Competing Interest

The authors declare that they have no known competing financial interests or personal relationships that could have appeared to influence the work reported in this paper.

Acknowledgements

This work is supported by the National Cancer Institute (R01CA227737, to C.-C.L.) and the National Science Foundation CAREER award (DMR1452390, to C.-C.L.). M.L.F. was supported by grants from the National Cancer Institute R01CA167291, R01CA167291-S1, U01HL143403, R01CA211098. M.L.F. was additionally supported by the Riley Children’s Foundation and the IUSCCC Pancreatic Cancer Working Group.

Supplementary materials

Supplementary material associated with this article can be found, in the online version, at doi:10.1016/j.actbio.2021.05.054.

References

[1] Y. Liu, Y. Jiang, M. Zhang, Z. Tang, M. He, W. Bu, Modulating hypoxia via nanomaterials chemistry for efficient treatment of solid tumors, Acc. Chem. Res. 51 (10) (2018) 2502–2511.
[2] Z. Tang, H. Zhang, Y. Liu, D. Ni, H. Zhang, J. Zhang, Z. Yao, M. He, J. Shi, W. Bu, Antiferromagnetic pyrite as the tumor microenvironment-mediated nanoplatform for self-enhanced tumor imaging and therapy, Adv. Mater. 29 (47) (2017) 1701683.
[3] M. Zhang, R. Song, Y. Liu, Z. Yi, X. Meng, J. Zhang, Z. Tang, Z. Yao, Y. Liu, X. Liu, W. Bu, Calcium-overload-mediated tumor therapy by calcium peroxide nanoparticles, Chem 5 (8) (2019) 2171–2182.
[4] F. Quiñonero, C. Mesas, K. Doello, L. Cabeza, G. Perazzoli, C. Jimenez-Luna, A.R. Rama, C. Melguizo, J. Prados, The challenge of drug resistance in pancreatic ductal adenocarcinoma: a current overview, Cancer Biol. Med. 16 (4) (2019) 688–699.
[5] S.K. Dougan, The pancreatic cancer microenvironment, Cancer J. 23 (6) (2017) 321–325.
[6] A.J. Rice, E. Cortes, D. Lachowski, B.C.H. Cheung, S.A. Karim, J.P. Morton, A. del Río Hernández, Matrix stiffness induces epithelial–mesenchymal transition and promotes chemoresistance in pancreatic cancer cells, Oncogenesis 6 (7) (2017) e352-e352.
[7] M. Weniger, K.C. Honselmann, A.S. Liss, The extracellular matrix and pancreatic cancer: a complex relationship, Cancers 10 (9) (2018) 316.
[8] N. Sato, S. Kohi, K. Hirata, M. Goggins, Role of hyaluronan in pancreatic cancer biology and therapy: once again in the spotlight, Cancer Sci. 107 (5) (2016) 569–575.
[9] B.A. Aguado, J.C. Grim, A.M. Rosales, J.J. Watson-Capps, K.S. Anseth, Engineering precision biomaterials for personalized medicine, Sci. Transl. Med. 10 (424) (2018) eaam8645.
[10] C.-C. Lin, M. Korc, Designer hydrogels: Shedding light on the physical chemistry of the pancreatic cancer microenvironment, Cancer Lett. 436 (2018) 22–27.
[11] R. Cruz-Acuña, A.J. García, Engineered materials to model human intestinal development and cancer using organoids, Exp. Cell Res. 377 (1) (2019) 109–114.
[12] M. Tang, Q. Xie, R.C. Gimple, Z. Zhong, T. Tam, J. Tian, R.L. Kidwell, Q. Wu, B.C. Prager, Z. Qiu, A. Yu, Z. Zhu, P. Mesci, H. Jing, J. Schimelman, P. Wang, D. Lee, M.H. Lorenzini, D. Dixit, L. Zhao, S. Bhargava, T.E. Miller, X. Wan, J. Tang, B. Sun, B.F. Cravatt, A.R. Muotri, S. Chen, J.N. Rich, Three-dimensional bioprinted glioblastoma microenvironments model cellular dependencies and immune interactions, Cell Res. 30 (10) (2020) 833–853.
[13] S.C. Allen, J.A. Widman, A. Datta, L.J. Suggs, Dynamic extracellular matrix stiffening induces a phenotypic transformation and a migratory shift in epithelial cells, Integr. Biol. 12 (6) (2020) 161–174.
[14] H.-Y. Liu, H.D. Nguyen, C.-C. Lin, Dynamic PEG–peptide hydrogels via visible light and FMN-induced tyrosine dimerization, Adv. Healthcare Mater. 7 (22) (2018) 1800954.
[15] M.R. Arkenberg, C.-C. Lin, Orthogonal enzymatic reactions for rapid crosslinking and dynamic tuning of PEG–peptide hydrogels, Biomater. Sci. 5 (11) (2017) 2231–2240.
[16] M.R. Arkenberg, H.D. Nguyen, C.-C. Lin, Recent advances in bio-orthogonal and dynamic crosslinking of biomimetic hydrogels, J. Mater. Chem. B 8 (35) (2020) 7835–7855.

[17] H.-Y. Liu, T. Greene, T.-Y. Lin, C.S. Dawes, M. Korc, C.-C. Lin, Enzyme-mediated stiffening hydrogels for probing activation of pancreatic stellate cells, Acta Biomater. 48 (2017) 258–269.
[18] M.R. Arkenberg, D.M. Moore, C.-C. Lin, Dynamic control of hydrogel crosslinking via sortase-mediated reversible transpeptidation, Acta Biomater. 83 (2019) 83–95.
[19] Z. Mũnoz, H. Shih, C.-C. Lin, Gelatin hydrogels formed by orthogonal thiol–norbornene photochemistry for cell encapsulation, Biomater. Sci. 2 (8) (2014) 1063–1072.
[20] T. Hozumi, T. Kageyama, S. Ohta, J. Fukuda, T. Ito, Injectable hydrogel with slow degradability composed of gelatin and hyaluronic acid cross-linked by Schiff's base formation, Biomacromolecules 19 (2) (2018) 288–297.
[21] K.E. Richards, A.E. Zeleniak, M.L. Fishel, J. Wu, L.E. Littlepage, R. Hill, Cancer-associated fibroblast exosomes regulate survival and proliferation of pancreatic cancer cells, Oncogene 36 (13) (2017) 1770–1778.
[22] H. Shih, T. Greene, M. Korc, C.-C. Lin, Modular and adaptable tumor niche prepared from visible light initiated thiol-norbornene photopolymerization, Biomacromolecules 17 (12) (2016) 3872–3882.
[23] D.R. Principe, M. Narbutis, S. Kumar, A. Park, N. Viswakarma, M.J. Dorman, S.D. Kamath, P.J. Grippo, M.L. Fishel, R.F. Hwang, D. Thummuri, P.W. Underwood, H.G. Munshi, J.G. Trevino, A. Rana, Long-term gemcitabine treatment reshapes the pancreatic tumor microenvironment and sensitizes murine carcinoma to combination immunotherapy, Cancer Res. 80 (15) (2020) 3101–3115.
[24] J. Sapudom, C.D. Müller, K.-T. Nguyen, S. Martin, U. Anderegg, T. Pompe, Matrix remodeling and hyaluronan production by myofibroblasts and cancer-associated fibroblasts in 3D collagen matrices, Gels 6 (4) (2020) 33.
[25] C.S. Ki, T.-Y. Lin, M. Korc, C.-C. Lin, Thiol-ene hydrogels as desmoplasia-mimetic matrices for modeling pancreatic cancer cell growth, invasion, and drug resistance, Biomaterials 35 (36) (2014) 9668–9677.
[26] J. Wu, Q. Zhao, C. Liang, T. Xie, Enzymatically degradable oxidized dextran—chitosan hydrogels with an anisotropic aligned porous structure, Soft Matter 9 (46) (2013) 11136–11142.
[27] T. Greene, T.-Y. Lin, O.M. Andrisani, C.-C. Lin, Comparative study of visible light polymerized gelatin hydrogels for 3D culture of hepatic progenitor cells, J. Appl. Polym. Sci. 134 (11) (2017).
[28] Y. Zheng, X. Xue, A.M. Resto-Irizarry, Z. Li, Y. Shao, Y. Zheng, G. Zhao, J. Fu, Dorsal-ventral patterned neural cyst from human pluripotent stem cells in a neurogenic niche, Sci. Adv. 5 (12) (2019) eaax5933.
[29] A. Suo, W. Xu, Y. Wang, T. Sun, L. Ji, J. Qian, Dual-degradable and injectable hyaluronic acid hydrogel mimicking extracellular matrix for 3D culture of breast cancer MCF-7 cells, Carbohydr. Polym. 211 (2019) 336–348.
[30] S.A. Fisher, P.N. Anandakumaran, S.C. Owen, M.S. Shoichet, Tuning the microenvironment: click-crosslinked hyaluronic acid-based hydrogels provide a platform for studying breast cancer cell invasion, Adv. Funct. Mater. 25 (46) (2015) 7163–7172.
[31] X. Xu, L.A. Gurski, C. Zhang, D.A. Harrington, M.C. Farach-Carson, X. Jia, Recreating the tumor microenvironment in a bilayer, hyaluronic acid hydrogel construct for the growth of prostate cancer spheroids, Biomaterials 33 (35) (2012) 9049–9060.
[32] L.A. Gurski, A.K. Jha, C. Zhang, X. Jia, M.C. Farach-Carson, Hyaluronic acid-based hydrogels as 3D matrices for in vitro evaluation of chemotherapeutic drugs using poorly adherent prostate cancer cells, Biomaterials 30 (30) (2009) 6076–6085.
[33] M.A. Anttila, R.H. Tammi, M.I. Tammi, K.J. Syrjänen, S.V. Saarikoski, V.-M. Kosma, High levels of stromal hyaluronan predict poor disease outcome in epithelial ovarian cancer, Cancer Res. 60 (1) (2000) 150–155.
[34] V.B. Lokeshwar, D. Rubinowicz, G.L. Schroeder, E. Forgacs, J.D. Minna, N.L. Block, M. Nadji, B.L. Lokeshwar, Stromal and epithelial expression of tumor markers hyaluronic acid and HYAL1 hyaluronidase in prostate cancer*, J. Biol. Chem. 276 (15) (2001) 11922–11932.
[35] P. Auvinen, R. Tammi, J. Parkkinen, M. Tammi, U. Ågren, R. Johansson, P. Hirvikoski, M. Eskelinen, V.-M. Kosma, Hyaluronan in peritumoral stroma and malignant cells associates with breast cancer spreading and predicts survival, Am. J. Pathol. 156 (2) (2000) 529–536.
[36] M.A. Jacobetz, D.S. Chan, A. Neesse, T.E. Bapiro, N. Cook, K.K. Frese, C. Feig, T. Nakagawa, M.E. Caldwell, H.I. Zecchini, M.P. Lolkema, P. Jiang, A. Kultti, C.B. Thompson, D.C. Maneval, D.I. Jodrell, G.I. Frost, H.M. Shepard, J.N. Skepper, D.A. Tuveson, Hyaluronan impairs vascular function and drug delivery in a mouse model of pancreatic cancer, Gut 62 (1) (2013) 112–120.
[37] X.-B. Cheng, S. Kohi, A. Koga, K. Hirata, N. Sato, Hyaluronan stimulates pancreatic cancer cell motility, Oncotarget 7 (4) (2015).
[38] H.-Y. Liu, M. Korc, C.-C. Lin, Biomimetic and enzyme-responsive dynamic hydrogels for studying cell-matrix interactions in pancreatic ductal adenocarcinoma, Biomaterials 160 (2018) 24–36.
[39] H.D. Nguyen, H.-Y. Liu, B.N. Hudson, C.-C. Lin, Enzymatic cross-linking of dynamic thiol-norbornene click hydrogels, ACS Biomater. Sci. Eng. 5 (3) (2019) 1247–1256.
[40] W.M. Gramlich, I.L. Kim, J.A. Burdick, Synthesis and orthogonal photopatterning of hyaluronic acid hydrogels with thiol-norbornene chemistry, Biomaterials 34 (38) (2013) 9803–9811.
[41] M.R. Arkenberg, N.H. Dimmitt, H.C. Johnson, K.R. Koehler, C.-C. Lin, Dynamic click hydrogels for xeno-free culture of induced pluripotent stem cells, Adv. Biosyst. 4 (11) (2020) 2000129.
[42] S.E. Holt, A. Rakoski, F. Jivan, L.M. Pérez, D.L. Alge, Hydrogel synthesis and stabilization via tetrazine click-induced secondary interactions, Macromol. Rapid Commun. 41 (14) (2020) 2000287.
[43] Y. Singh, D. Gao, Z. Gu, S. Li, K.A. Rivera, S. Stein, S. Love, P.J. Sinko, Influence of molecular size on the retention of polymeric nanocarrier diagnostic agents in breast ducts, Pharm. Res. 29 (9) (2012) 2377–2388.
[44] J.K. Armstrong, R.B. Wenby, H.J. Meiselman, T.C. Fisher, The hydrodynamic radii of macromolecules and their effect on red blood cell aggregation, Biophys. J. 87 (6) (2004) 4259–4270.
[45] R.H. Tromp, A.R. Rennie, R.A.L. Jones, Kinetics of the simultaneous phase separation and gelation in solutions of dextran and gelatin, Macromolecules 28 (12) (1995) 4129–4138.
[46] M.F. Butler, M. Heppenstall-Butler, Phase separation in gelatin/dextran and gelatin/maltodextrin mixtures, Food Hydrocolloids. 17 (6) (2003) 815–830.
[47] M.W. Edelman, E. van der Linden, E. de Hoog, R.H. Tromp, Compatibility of gelatin and dextran in aqueous solution, Biomacromolecules 2 (4) (2001) 1148–1154.
[48] B.P. Toole, Hyaluronan: from extracellular glue to pericellular cue, Nat. Rev. Cancer 4 (7) (2004) 528–539.
[49] L.A. Gurski, X. Xu, L.N. Labrada, N.T. Nguyen, L. Xiao, K.L. van Golen, X. Jia, M.C. Farach-Carson, Hyaluronan (HA) interacting proteins RHAMM and hyaluronidase impact prostate cancer cell behavior and invadopodia formation in 3D HA-based hydrogels, PLoS One 7 (11) (2012) e50075.
[50] A. Domenichini, J.S. Edmands, A. Adamska, R.-R. Begicevic, S. Paternoster, M. Falasca, Pancreatic cancer tumorspheres are cancer stem-like cells with increased chemoresistance and reduced metabolic potential, Adv. Biol. Regulat. 72 (2019) 63–77.
[51] J.P. Thiery, Epithelial–mesenchymal transitions in tumour progression, Nat. Rev. Cancer 2 (6) (2002) 442–454.
[52] F. Strutz, M. Zeisberg, F.N. Ziyadeh, C.-Q. Yang, R. Kalluri, G.A. Müller, E.G. Neilson, A. Renziehausen, Z. Sisic, Role of basic fibroblast growth factor-2 in epithelial-mesenchymal transformation, Kidney Int. 61 (5) (2002) 1714–1728.
[53] Y. Kim, S. Kumar, CD44-mediated adhesion to hyaluronic acid contributes to mechanosensing and invasive motility, Mol. Cancer Res. 12 (10) (2014) 1416–1429.
[54] J.-I. Choi, S.I. Jang, J. Hong, C.H. Kim, S.S. Kwon, J.S. Park, J.-B. Lim, Cancer-initiating cells in human pancreatic cancer organoids are maintained by interactions with endothelial cells, Cancer Lett. 498 (2021) 42–53.
[55] V. Assmann, C. Fieber, P. Herrlich, M. Hofmann, C.C. Termeer, T. Ahrens, J.C. Simon, CD44 is the principal mediator of hyaluronic-acid-induced melanoma cell proliferation, J. Invest. Dermatol. 116 (1) (2001) 93–101.
[56] M.F.B. Nielsen, M.B. Mortensen, M.D. Sørensen, M. Wirenfeldt, B.W. Kristensen, H.D. Schrøder, P. Pfeiffer, S. Detlefsen, Spatial and phenotypic characterization of pancreatic cancer-associated fibroblasts after neoadjuvant treatment, Histol. Histopathol. 35 (8) (2020) 811–825.
[57] H.M. Kim, Y.K. Lee, J.S. Koo, Expression of CAF-related proteins is associated with histologic grade of breast phyllodes tumor, Dis. Markers 2016 (2016) 4218989.
[58] K. Pietras, J. Pahler, G. Bergers, D. Hanahan, Functions of paracrine PDGF signaling in the proangiogenic tumor stroma revealed by pharmacological targeting, PLoS Med. 5 (1) (2008) e19.
[59] T. Kawase, Y. Yasui, S. Nishina, Y. Hara, I. Yanatori, Y. Tomiyama, Y. Nakashima, K. Yoshida, F. Kishi, M. Nakamura, K. Hino, Fibroblast activation protein-α-expressing fibroblasts promote the progression of pancreatic ductal adenocarcinoma, BMC Gastroenterol. 15 (1) (2015) 109.
[60] G.M. Son, M.-S. Kwon, D.-H. Shin, N. Shin, D. Ryu, C.-D. Kang, Comparisons of cancer-associated fibroblasts in the intratumoral stroma and invasive front in colorectal cancer, Medicine (Baltimore). 98 (18) (2019) e15164.
[61] D. Öhlund, A. Handly-Santana, G. Biffi, E. Elyada, A.S. Almeida, M. Ponz-Sarvise, V. Corbo, T.E. Oni, S.A. Hearn, E.J. Lee, I.I.C. Chio, C.-I. Hwang, H. Tiriac, L.A. Baker, D.D. Engle, C. Feig, A. Kultti, M. Egeblad, D.T. Fearon, J.M. Crawford, H. Clevers, Y. Park, D.A. Tuveson, Distinct populations of inflammatory fibroblasts and myofibroblasts in pancreatic cancer, J. Exp. Med. 214 (3) (2017) 579–596.
[62] C. Benzing, H. Lam, C.M. Tsang, A. Rimmer, Y. Arroyo-Berdugo, Y. Calle, C.M. Wells, TIMP-2 secreted by monocyte-like cells is a potent suppressor of invadopodia formation in pancreatic cancer cells, BMC Cancer 19 (1) (2019) 1214.